The data processing pipelines for the Herschel/SPIRE Imaging Fourier Transform Spectrometer

Trevor R. Fulton[a*], Jean-Paul Baluteau[b], George Bendo[c], Dominique Benielli[b], Rene Gastaud[d], Matt Griffin[e], Steve Guest[f], Peter Imhof[a], Tanya L. Lim[f], Nanyao Lu[g], David A. Naylor[h], Pasquale Panuzzo[d], Edward Polehampton[f,h], Arnold Schwartz[g], Christian Surace[b], Bruce M. Swinyard[f], Kevin Xu[g]

[a]Blue Sky Spectroscopy Inc., 9 - 740 4 Avenue South, Lethbridge, T1J 0N9, Canada;
[b]Laboratoire d'Astrophysique de Marseille, Marseille, France, 13388;
[c]Astrophysics Group, Imperial College, London, United Kingdom, SW7 2AZ;
[d]Laboratoire AIM, CEA-Saclay, France, 91191;
[e]School of Physics and Astronomy, Cardiff University, Cardiff, United Kingdom, CF24 3AA;
[f]Space Science and Technology Department, Rutherford Appleton Laboratory, Didcot, United Kingdom, OX11 0QX;
[g]Infrared Processing and Analysis Center, California Institute of Technology, Pasadena, USA,91125;
[h]Institute for Space Imaging Sciences, University of Lethbridge, Lethbridge, T1K 3M4, Canada

ABSTRACT

We present an update to the data processing pipelines that generate calibrated spectral data products from the Spectral and Photometric Imaging Receiver (SPIRE), one of three scientific instruments onboard the European Space Agency's Herschel Space Observatory launched on 14 May 2009. The pipelines process telemetry from SPIRE's imaging Fourier Transform Spectrometer (FTS) taken in point source, jiggle- and raster-map observing modes, producing calibrated spectra in low-, medium-, high-, and mixed low- and high-spectral resolution. While the order and algorithms of the data processing modules in the spectrometer pipelines remain for the most part unchanged compared to their pre-launch status, some improvements and optimizations have been realized through the analysis of data from the performance verification and science demonstration phases of the mission. The data processing pipelines for the SPIRE FTS as of the beginning of the routine phase of the Herschel mission are presented in their entirety, with more detailed descriptions reserved for those elements that have changed since launch, in particular the first- and second-level correction steps for glitches, the step that corrects for clipped samples, and the process by which Level-1 spectral data are converted to Level-2 products. In addition, we discuss some of the challenging aspects still faced by the automated processing pipelines, such as the removal of the contributions from the Herschel telescope and SPIRE instrument, and the relative spectral response correction and flux conversion steps.

Keywords: Herschel, SPIRE, Imaging Fourier transform spectroscopy, Data processing, Pipeline

1. INTRODUCTION

The data processing pipelines for the Spectral and Photometric Imaging Receiver[1],[2] (SPIRE) Fourier transform spectrometer (FTS) contain processing modules commonly used to process FTS data, such as phase correction and the Fourier transform. The SPIRE FTS pipelines also contain processing steps unique to SPIRE, such as the correction for the thermal variations of the Herschel telescope and spectrometer itself.

The SPIRE FTS pipelines have been designed to be consistent with the astronomical observation templates[3] (AOTs) that are available to the users of the SPIRE spectrometer. The final data products generated by the spectrometer pipelines will in all cases consist of spectral data, but the format of the data products depends on the AOT. Point source spectra for the two target detectors are produced for single pointing sparse sampling observations; hyperspectral cubes that contain two spatial dimensions representing the astronomical region under study and one spectral dimension, are produced for mapping observations.

*Email: trevor.fulton@blueskyinc.ca; Telephone: (403) 317-1273; Fax: (403) 317-1273; www.blueskyinc.ca

Space Telescopes and Instrumentation 2010: Optical, Infrared, and Millimeter Wave,
edited by Jacobus M. Oschmann Jr., Mark C. Clampin, Howard A. MacEwen, Proc. of SPIE
Vol. 7731, 773134 · © 2010 SPIE · CCC code: 0277-786X/10/$18 · doi: 10.1117/12.858282

1.1 Spatial Sampling

The spatial sampling in the final hyperspectral cubes for mapping observations depends on a combination of the number of requested raster positions of the Herschel telescope and the number of jiggle positions of the SPIRE Beam Steering Mirror (BSM) selected. The number of Herschel telescope raster positions, n, depends on the observing area requested and is limited by the maximum observing time for one AOT (18 hours[3]). A list of the spatial sampling options available to observers is shown in Table 1.

Table 1: SPIRE spectrometer spatial sampling options.

Spatial Sampling	Astronomical Observation Template	Number of Herschel Telescope Raster Positions	Number of BSM Jiggle Positions	Total Number of Pointing Positions	Pixel Size [arcsec] SSW Band	Pixel Size [arcsec] SLW Band
Single, Sparse	SOF1	1	1	1	N/A	N/A
Single, Intermediate	SOF2	1	4	4	19.0	35.0
Single, Full	SOF2	1	16	16	9.5	17.5
Raster, Sparse	SOF1	n	1	n	38.0	70.0
Raster, Intermediate	SOF2	n	4	4n	19.0	35.0
Raster, Full	SOF2	n	16	16n	9.5	17.5

1.2 Spectral Resolution

A SPIRE FTS observation building block is defined as a set of equal-length scans of the SPIRE Spectrometer Mechanism (SMEC) at a single pointing position of the Herschel telescope and SPIRE BSM. The spectral resolution of these scans is determined by the maximum optical path difference (OPD) that the instrument can achieve by displacing the SMEC from the point of symmetry, or zero path difference (ZPD). The spectral resolution options available to astronomical observers for the SPIRE FTS are shown in Table 2[3],[10].

Table 2: SPIRE spectrometer spectral resolution options.

Spectral Resolution	Scan Length (OPD) [cm]	Spectral Resolution [cm^{-1}]
Low	0.60	0.83
Medium	2.08	0.240
High	12.56	0.0398

1.3 SPIRE Spectrometer Pipelines

The block diagram of the SPIRE spectrometer data processing pipelines is shown in Figure 1. The structure of the data processing pipelines follows the observation building blocks. This structure is designed to allow the processing modules that modify the signal data of the SPIRE spectrometer detectors to take advantage of symmetries and redundancies that are present for a series of FTS scans of the same astronomical target.

In this paper we describe the SPIRE spectrometer data processing pipelines in two sections. The first of these (Section 2) describes the modules that are common to all observing modes and pipelines -- the building block pipeline -- which produces Level-1 interferogram and spectral products (Figure 1). The second describes the processing steps that convert the Level-1 spectral products, either through spatial combination to produce Level-2 hyperspectral cubes for raster and/or jiggle observations, or by spectral conversion to produce a Level-2 Point Source spectrum for single pointing sparse observations (Section 3).

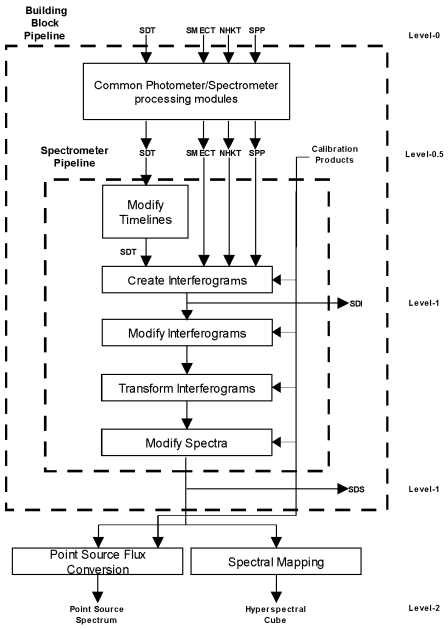

Figure 1: SPIRE FTS data processing block diagram.

2. SPIRE SPECTROMETER BUILDING BLOCK PIPELINE

The portion of the SPIRE spectrometer data processing pipeline described here operates on one observation building block at a time. The building block pipeline consists of six major processing groups (Figure 1). The overall structure of the building block pipeline remains as it was prior to launch.

1. **Common Photometer/Spectrometer Processing modules.** These processing steps are common to both the SPIRE spectrometer and photometer pipelines and are presented elsewhere[4].
2. **Modify Timelines.** These processing modules perform operations on detector signals that are time-dependent and are described in Section 2.1.
3. **Create Interferograms.** This processing step merges the timelines of the spectrometer detectors and spectrometer mechanism into interferograms. This step produces a Level-1 Spectrometer Detector Interferogram product and is described in Section 2.2.
4. **Modify Interferograms.** The processing modules in this group perform operations on the spectrometer detector interferograms. These operations differ from those in the "**Modify Timelines**" group in that they are designed to act on signals that are a function of OPD rather than signals that are a function of time. These processing modules are described in Section 2.3.
5. **Transform Interferograms.** This processing step transforms the interferograms into a set of spectra, resulting in a Level-0.5 Spectrometer Detector Spectrum product described in Section 2.4.
6. **Modify Spectra.** The processing modules in this group perform operations on spectra. The steps in this category combine to produce a Level-1 Spectrometer Detector Spectrum product and are described in Section 2.5.

2.1 Detector Timeline Modifications

After application of the processing steps common to both the photometer and spectrometer detectors timelines[4], the raw samples for each one of the 66 spectrometer detectors, labeled *i*, will have been converted into RMS voltage timelines, $V_{RMS\text{-}i}(t)$. These quantities are contained in the Level-0.5 Spectrometer Detector Timeline Product (SDT).

The processing modules described in the following sections are applied to the timelines for each spectrometer detector. Each of the processing steps contained in this processing block (Figure 2) accepts a Level-0.5 SDT product as input and delivers an SDT product as output.

The major modifications to this processing block since launch consist of a change to the processing order within the block and the addition of an extra processing step. The time domain phase correction module (Section 2.1.6) now follows the corrections for detector non-linearity and fluctuations of the detector bath temperature (Sections 2.1.3 and 2.1.4). Also, a step that corrects detector timeline samples which have been clipped by the limited dynamic range of the read-out electronics has been added (Section 2.1.5).

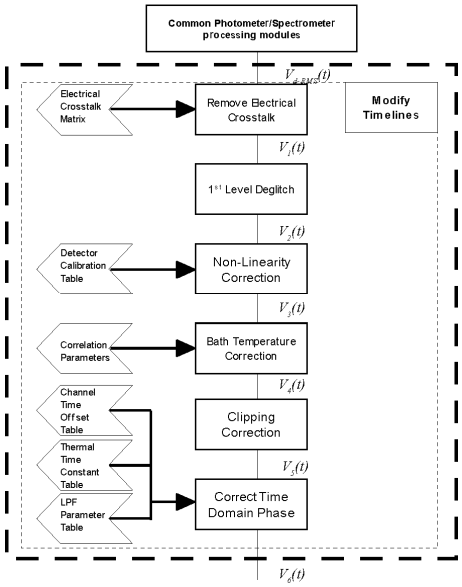

Figure 2: Timeline modification section of the SPIRE Spectrometer building block pipeline.

2.1.1 Electrical Crosstalk

Before launch, it was anticipated that the spectrometer detector timelines would contain contributions that depend on the signals from other detectors due to electrical crosstalk. Such contributions would then be removed from the SPIRE

spectrometer detector timelines by multiplication of a crosstalk matrix. Notwithstanding the analysis of the data from the early post-launch phases that has shown very limited evidence for significant crosstalk, the electrical crosstalk correction step has been retained in case such an effect manifests itself over the course of the routine phase of the mission. For the time being, however, this step applies a null subtraction to the spectrometer detector timelines.

2.1.2 First-level Deglitching

Glitches due to cosmic ray hits or other events in the detectors are removed from the timelines of the spectrometer detectors using an algorithm based on a wavelet-based local regularity analysis[5]. This process is composed of two steps: the first detects glitch signatures over the measured signal; the second locally reconstructs the signal timeline by removing the glitch signature.

1. **Glitch Identification.** Glitches are detected in the input SDT product by continuous wavelet analysis and a subsequent analysis of the modulus maxima lines, assuming that the glitch signature is similar to the signature of a Dirac delta function.
2. **Glitch Removal.** Each glitch flagged by the preceding step and its nearest neighboring samples are replaced by a localized eighth-order polynomial fit to the detector timeline.

Early in the performance verification phase of the Herschel mission, it became clear that the frequency and amplitude of glitches in the spectrometer detector timelines is much greater in-flight than pre-launch. This placed particular importance on both this module and the second-level deglitching module (Section 2.3.2). After evaluation of the observational data from the performance verification phase, the parameters for the first-level deglitching module were optimized to identify and correct glitches with larger amplitudes, while relying on the second-level deglitching to identify and correct the smaller glitches.

2.1.3 Detector Non-linearity Correction

The next step in the processing pipelines is designed to account for the well known non-linear response of SPIRE detector bolometers. As was the case before launch, the form of this correction is a function that is dependent on the amplitude of the recorded signal as follows:

$$V_{3-i}(t) = \int_{V_0}^{V_{2-i}} \frac{f(V)}{f(V_r)} dV \,, \tag{1}$$

where $f(V)$, the real detector responsivity, V_r is a reference voltage, and V_0 is a fixed bolometer voltage. The normalized value of $f(V)$ is derived as:

$$\frac{f(V)}{f(V_r)} = K_1 + \frac{K_2}{V - K_3} \,. \tag{2}$$

The values for V_0, K_1, K_2, and K_3 (and their uncertainties) for each detector are stored in a calibration tables supplied as input to this processing module. Separate calibration tables, populated with information based on in-flight observations, are used for each of the nominal and bright source detectors settings.

2.1.4 Bath Temperature Correction

To first order, bath temperature fluctuations will influence, coherently, all detectors in an array. Each of the two detector arrays of the SPIRE spectrometer contains two bolometers dedicated to measuring the temperature of the detector array. These thermometers are used to create a correction timeline for each detector, $V_{th\text{-}i}(t)$. This timeline is then subtracted from that detector's signal timeline, $V_{4\text{-}i}(t)$.

The output of this module is a set of spectrometer detector voltage timelines corrected for correlated low-frequency thermal drifts.

2.1.5 Clipping Correction

The purpose of this processing step is to correct those signal samples in the input SDT timelines that were clipped due to the limited dynamic range of the detector ADCs. Clipped samples are essentially signal samples with incorrect values that, if left uncorrected, will introduce errors when the timelines are converted into interferograms (Section 2.2).

The process by which clipped timelines are corrected is described below.

1. **Identify the clipped samples in the SDT timelines.** The processing modules common to both the SPIRE spectrometer and photometer contain a step whereby detector samples whose raw ADC values are either 0 or 2^{16}-1 (65535) are flagged as having been clipped.
2. **Interpolate the modified SDT timeline.** A polynomial of degree eight is applied to the five points before and after those samples identified as being clipped.
3. **Replace the SDT timeline**. Samples that had been identified as clipped in the original detector timeline, $V_{4\text{-}i}(t_k)$, are replaced with the results of the polynomial fit, $V_{fit\text{-}i}(t_k)$.

$$V_{5-i}(t_k) = V_{fit-i}(t_k). \tag{3}$$

4. **Propagate the remainder of the SDT timelines.** Samples that were not identified as being clipped, $V_{4\text{-}i}(t_j)$, are simply propagated to the resultant timeline, $V_{5\text{-}i}(t_j)$.

$$V_{5-i}(t_j) = V_{fit-i}(t_j). \tag{4}$$

Before launch, it was anticipated that the voltage offsets for the spectrometer detectors could be optimized so as to minimize the frequency of clipped samples. Analysis of the data from the performance verification and science demonstration phases revealed that, while it is possible to choose a bias voltage to minimize the number of clipped samples for the central detectors of each array for sources of nominal brightness[3], no such optimization is possible for brighter sources nor is such an optimization possible for all detectors simultaneously regardless of the brightness of the source. As a result, it was necessary to develop a processing step to correct for this phenomenon.

2.1.6 Time Domain Phase Correction

Next, the measured spectrometer detector timelines are corrected for the time delay induced by the combined effects of the low pass filters (LPFs) in the read-out electronics[6] and the detector thermal response. As was the case before launch, this correction involves characterizing the delay in the frequency domain, $\varphi_{Total\text{-}i}(\omega)$, and then correcting the timelines in the time domain by way of convolution with the inverse transform of this phase delay, $PCF_i(t)$, as in eq. 6 below.

$$PCF_i(t) = FT^{-1}\left[e^{-i\varphi_{Total-1}(\omega)}\right], \tag{5}$$

$$V_{6-i}(t) = V_{5-1}(t) \otimes PCF_i(t). \tag{6}$$

2.2 Interferogram Creation

The pipeline modules listed to this point describe the operations on the Level-0.5 timelines of the spectrometer detectors. Three additional Level-0.5 timelines are required for the next step in the common spectrometer data processing pipeline. These are: the Spectrometer Mechanism timeline product (SMECT); the Nominal Housekeeping timeline product (NHKT); and the SPIRE Pointing timeline product (SPP) (see Figure 1).

2.2.1 Interferogram Creation

A Fourier transform spectrometer measures interferograms, i.e. detector signals as a function of OPD. In the case of the SPIRE FTS, the sampling of the SPIRE spectrometer detectors and the spectrometer mechanism is decoupled; the two subsystems are sampled at different rates and at different times. The interferogram creation step links the timelines of the Spectrometer Mechanism with the Spectrometer Detector timelines. The SMEC positions, to which the spectrometer detector signal samples are linked, are converted to an equidistant grid of OPD positions in order to ensure accurate transformation of the interferogram with the Discrete Fourier Transform. The interferogram creation module of the SPIRE spectrometer pipeline performs these tasks in two steps: interpolation of the SMEC timeline; and merging of the Spectrometer Detector and SMEC timelines. As the algorithms employed by the interferogram creation processing module have not been modified from their pre-launch state, only a summary of these steps is presented here.

1. **Interpolation of the SMEC timeline.** The spectrometer mechanism timeline is converted from one that is non-uniform in position to one that is uniform in position by first establishing, for all of the output

interferograms, a common set of regularly-spaced optical path difference positions onto which the measured SMEC positions will be mapped. The SMEC positions are mapped, for each spectrometer detector, taking into account the position of zero path difference unique to each detector, ZPD_i, and a scaling factor, f_i, again unique each detector, that takes the off-axis obliquity effect into account. Finally, the sample times when the spectrometer mechanism reached the regularly-spaced OPD positions are determined through cubic spline interpolation.

2. **Merge the spectrometer detector and the mapped SMEC timelines.** This step combines the signal samples from the timeline of a given spectrometer detector, $V_{6\text{-}i}(t_i)$, with the regularly-spaced OPD positions for each scan for each detector. As each of the signal and position vectors are functions of time, this process involves interpolation -- again using a cubic spline -- of the detector signal timelines, $V_{6\text{-}i}(t_i)$, onto the times when, for the same detector, i, the SMEC reached the positions in the regularly-spaced optical path difference vector.

The process outlined above is repeated for all spectrometer detectors for each scan of the observation building block. In addition, the mean value of the pointing for each detector, $P_{n\text{-}i}(t)$, as derived from the input SPP for the observation building block is assigned to the each interferogram output SDI product.

The data product that results from this processing step is a Level-1 Spectrometer Detector Interferogram (SDI) product that will be made available to observers.

2.3 Interferogram Modification

The pipeline modules described in this section perform operations on the interferograms created in the previous step. Each of the processing steps contained in this processing block accept an SDI product as input and deliver an SDI product as output (Figure 3).

Prior to launch the first processing step in this block was the correction for the contributions of the Herschel telescope and the SPIRE instrument (Section 2.3.3). This step has since been moved to follow the Baseline correction (Section 2.3.1) and Second-level deglitching steps (Section 2.3.2) as analysis of the in-flight data has shown that processing the spectrometer data in this manner yielded more consistent results.

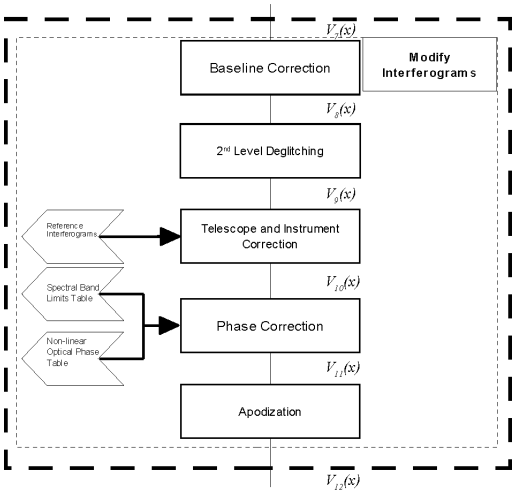

Figure 3: Interferogram modification section of the SPIRE Spectrometer building block pipeline.

2.3.1 Baseline Correction

Despite the efforts to remove correlated drifts in the detector timelines (Section 2.1.4), the measured interferograms may still display a varying baseline due to perturbations which did not occur uniformly across the detector array. The baseline correction algorithm evaluates and removes, on a detector-by-detector and scan-by-scan basis, the offset portion of the measured interferograms, $V_{7\text{-}i}(x)$. Prior to launch, the interferogram baselines were evaluated by way of a fourth-order polynomial fitted to the measured interferogram. Analysis of the in-flight data has shown that a fit based on the low frequency spectral components produced results with a higher signal-to-noise ratio, in particular for detectors in the SLW array. The current algorithm determines the interferogram baseline from that portion of the measured interferogram whose spectral components are below 4cm^{-1} (eq. 7).

$$V_{Baseline-i}(x) = FT^{-1}\left[FT\left[V_{8-i}(x)\right]_{\sigma=4}^{\sigma=0}\right]. \tag{7}$$

The baselines as evaluated by eq. 7 are then subtracted from the input interferograms to derive the corrected interferograms,

$$V_{8-i}(x) = V_{7-i}(x) - V_{Baseline-i}(x)\,. \tag{8}$$

2.3.2 Second-level Deglitching

The second-level deglitching step is responsible for identifying and correcting any glitches not corrected by first-level deglitching (Section 2.1.2). This step relies on the principle that repeated FTS measurements of the same astronomical source should not deviate from one another beyond random noise. Glitches may then be identified for each spectrometer detector as those that, for a given OPD position, deviate by a given threshold from corresponding samples taken from all other scans in the same building block.

Based on a combination of pre-launch and performance verification phase data, the most effective statistical metric found for identifying second-level glitches is the windowed median absolute deviation algorithm[7]. This algorithm first computes, for a given detector, the standard deviation at each OPD position from all of the measured interferograms. A given OPD position, x, is considered to contain a glitch if its standard deviation differs by more than a pre-determined threshold, d, from median deviation, $MAD_w()$, of a window, w, of its neighboring samples.

$$\partial V_{8-i}(x_k) - MEDIAN_w(\partial V_{8-i}(x)) > d \times 1.4826 \times MAD_w\left(\partial V_{8-i}(x_l)\right), \tag{9}$$

$$MAD_w(\partial V_{8-i}(x_k)) = MAD\left(\partial V_{8-i}(x_{k-\frac{w-1}{2}}), \ldots, \partial V_{8-i}(x_{k+\frac{w-1}{2}})\right). \tag{10}$$

The samples that are identified as glitches are then replaced. The value of the replacement sample for a glitch identified at a given position for a given spectrometer detector is determined by the average of the samples from the other observed interferograms at that position,

$$V_{j-9-i}(x_k) = \frac{1}{N_{Scans} - 1} \sum_{n=1, n\neq j}^{N_{Scans}} V_{n-8-1}(x_k). \tag{11}$$

All second-level deglitching methods rely on a statistical analysis of the measured interferograms and require at least three interferograms per building block to be effective.

2.3.3 Telescope and Instrument Correction

At this point of the processing chain, the voltages recorded in the interferograms consist of a contribution from the observed astronomical source as well as the signals from both the Herschel telescope and the SPIRE instrument itself. The sum total of these contributions may be expresses as below:

$$V_{9-i}(x) = V_{9-Source-i}(x) + V_{9-Telescope-i}(x) + V_{9-Instrument-i}(x). \tag{12}$$

Throughout the mission, calibration observations are performed by observing a region of space known to have low emission. In these cases, the resultant reference interferograms, $V_{9\text{-}ref\text{-}i}(x)$, only contain contributions from the Herschel telescope and SPIRE instrument:

$$V_{9-ref-i}(x) = V_{9-Telescope-ref-i}(x) + V_{9-Instrument-ref-i}(x). \tag{13}$$

The contributions from the Herschel telescope and the SPIRE instrument components from the measured are removed from the on-source observation by subtracting the interferograms derived from the reference observations,

$$\begin{aligned} V_{10-i}(x) &= V_{9-i}(x) + V_{9-ref-i}(x) \\ &= V_{9-Source-i}(x) \end{aligned}. \tag{14}$$

The result shown in eq. 14 is valid if the thermal state of the Herschel telescope and SPIRE instrument remains the same during both the reference and the on-source observation. Analysis of the SPIRE spectrometer data from the performance verification and science demonstration phases indicates that thermal variations in both of these components is occurring. Moreover, it has been found that these thermal variations are large enough to impact the quality of the final spectra, with the thermal variations in the instrument primarily affecting the long wavelength spectra and thermal variations in the telescope variations primarily the short wavelength spectra. A correction step that takes these variations into account is currently under investigation. In the meantime, specialized interactive processing is required to account for these effects.

2.3.4 Phase Correction

The phase correction module, designed to remove any remaining asymmetries from the recorded interferograms, is separated into two components: the first step identifies any phase or asymmetry present in the input interferograms; the second step applies a correction to the input interferograms by removing this phase. The algorithm employed by this processing module to identify the interferogram phase is identical to that used before launch, with the exception that now, instead of fitting a fourth-order polynomial to the measured phase, a second-order polynomial is used as the fitting function (eq. 15). Correction of the input interferograms then proceeds as before launch, by way of a convolution of the input interferograms with the inverse transform of the negative of the fitted phase (eqs. 16, 17).

$$\varphi_{fit-i}(\sigma) = a_i + b_i \sigma_{Measured} + c_i \sigma^2_{Measured}\Big|_{\sigma_{Low}}^{\sigma_{High}}, \tag{15}$$

$$PCF_i(\sigma) = e^{-i\varphi_{fit-i}(\sigma)}, \tag{16}$$

$$V_{11-i}(x) = V_{10-i}(x) \otimes FT^{-1}\left[PCF_i(\sigma)\right]. \tag{17}$$

2.3.5 Apodization

If the source signal contains features at or near the resolution of the spectrometer, the instrument line shape of the FTS, results the well known sinc function, which introduces secondary oscillatory lobes in the derived spectra. An apodization function can be applied to the recorded interferograms to mitigate this effect at the cost of reducing the resolution of the resultant spectrum. The spectrometer pipelines therefore offer observers two sets of spectra; one that has been apodized with a Hanning function, and one that has not.

$$V_{12-Unapodized-i}(x) = V_{11-i}(x), \tag{18a}$$

$$V_{12-Apodized-i}(x) = V_{11-i}(x) \times Hannning_i(x). \tag{18b}$$

While the apodization function chosen for the standard processing pipeline is the Hanning[8] function, a number of apodizing functions that allow for an optimal trade-off between reduction in the secondary maxima and reduced resolution[9] are available to be used in interactive processing.

2.4 Spectrum Creation

At this point in the spectrometer pipeline, all required corrections have been applied to the measured interferograms in order to remove any asymmetries. The Fourier transform is now applied to transform the interferograms for each detector, $V_{n\text{-}m\text{-}i}(x)$, into spectra, $B_{n\text{-}m\text{-}i}(\sigma)$, and any further corrections in the spectrometer pipelines take place in the spectral domain.

2.4.1 Fourier Transform

The Fourier Transform processing module performs two important functions in the spectrometer pipelines: first, the module ensures that the sampling intervals of the resultant spectra are such that comparisons of the spectra acquired at different resolutions can be readily made; second, the module transforms the set of input interferograms into a set of spectra.

1. **Establish the desired spectral sampling interval.** The desired spectral sampling interval is achieved by padding the input interferograms with zeroes. As noted above, the processing steps up to now have rendered the interferograms symmetric about the position of ZPD (Section 2.3). As such, only those samples that are greater than or equal to the position of ZPD need to be considered:

$$V_{12-ZP-i}(x) = V_{12-i}(x)\Big|_0^L, 0\Big|_L^{L_{ZP}}, \tag{19}$$

$$\Delta\sigma_{ZP} = \frac{1}{2L_{ZP}}, \tag{20}$$

where L is the unpadded interferogram length and L_{ZP} and $\Delta\sigma_{ZP}$ are the padded interferogram length and desired spectral sampling intervals, respectively. The SPIRE spectrometer AOTs[3] provide three spectral resolution options to observers. The values to which L_{ZP} and $\Delta\sigma_{ZP}$ are set depend on the commanded resolution and are given in Table 3, below.

2. **Transform the padded interferograms.** The Discrete Fourier Transform is then applied to each of the padded interferograms given by eq. 19 to produce spectra for each detector and for each scan of the spectrometer mechanism:

$$B_{13-ZP-i}(\sigma_k) = \sum_{x_n=0}^{L_{ZP}-1} V_{12-ZP-i}(x_n) e^{-\frac{i2\pi\sigma_k x_n}{L_{ZP}}} \quad . \tag{21}$$

Table 3: Spectral sampling intervals for three SPIRE spectral resolution observing options.

Commanded Spectral Resolution	Sampling Interval, Δx (OPD) [μm]	Nyquist Wavenumber, $\sigma_{Nyquist}$ [cm^{-1}]	Padded scan length, L_{zp} (OPD) [cm]	Spectral Sampling Interval, $\Delta\sigma_{ZP}$ [cm^{-1}]
Low	25	200	2.0	0.25
Medium	25	200	10.0	0.05
High	25	200	50.0	0.01

2.5 Spectral Modification

The pipeline modules described in this section apply corrections best performed in the spectral domain. Several changes have been made to this section of the spectrometer building block pipeline from its state pre-launch. Most notable among these changes are that spectral averaging is now the first step in this block (see Figure 4) and the relative spectral response and flux conversion steps have now been merged into a single processing module. The end result of these processing steps remains the same as it was before launch; a Level-1 Spectrometer Detector Spectrum product that contains a single, flux-calibrated, average spectrum for each spectrometer detector, $I_i(\sigma)$, is produced.

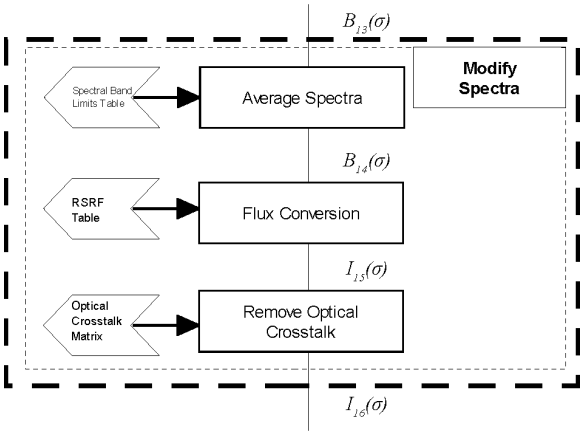

Figure 4: Spectral modification section of the SPIRE Spectrometer building block pipeline.

2.5.1 Spectral Averaging

This step of the spectrometer building block pipeline computes the average of the spectral intensities for each detector. The module first identifies, on a wavenumber-by-wavenumber basis, statistical outliers using the same method as in second-level deglitching (Section 2.3.2) and then computes the average of the spectral intensities across the scans, n, among the remaining samples, $B_{n\text{-}12\text{-}i}(\sigma_k)$,

$$\overline{B_{13-i}(\sigma_k)} = \frac{1}{N_{Scans}} \sum_{n=1}^{N_{Scans}} B_{n-12-i}(\sigma_k) \, . \tag{22}$$

The uncertainty in the average spectral intensity is set as the standard deviation of the spectral components,

$$\partial B_{13-i}(\sigma_k) = \sqrt{\frac{1}{N_{Scans}-1} \sum_{n=1}^{N_{Scans}} \left(B_{n-12-i}(\sigma_k) - \overline{B_{12-i}(\sigma_k)} \right)^2} \quad . \tag{23}$$

2.5.2 Extended Source Spectral Response Correction and Flux Conversion

The response of the SPIRE spectrometer detector subsystem depends on the wavelength and on the extent of the incoming radiation -- the response for point-like sources differs from that for sources that fill the detector's field of view,

as confirmed by in-flight observations[10],[11]. This module performs two functions simultaneously: it removes from the measured spectrum of each detector in the input SDS product the relative spectral response function (RSRF) for that particular detector; and it converts the spectral intensities from quantities with units of Volts/(cm^{-1}) to optical power quantities with units of Watts/m^2/sr/Hz. At this stage, since the morphology of the astronomical source is unknown, the extended source correction is applied. The correction that is to be applied is given below:

$$I_{14-i}(\sigma) = B_{13-i}(\sigma) \times \frac{f_{i-Extended}(\sigma)}{RSRF_{i-Extended}(\sigma)}. \quad (24)$$

The extended source RSRF correction and flux conversion curves, $f_{i\text{-}Extended}(\sigma)/RSRF_{i\text{-}Extended}(\sigma)$, are derived from a combination of the multiple calibration observations of the Herschel telescope and a thermal model of the Herschel telescope's primary and secondary mirrors[10],[12].

2.5.3 Removal of Optical Crosstalk

Optical crosstalk is defined as power from the astronomical source that should be incident on one detector, but is actually received by another. Prior to launch, it was anticipated that even if a source is on-axis for a given detector, a small fraction of the source power will be incident on the neighboring detectors due to diffracted energy that is challenging to model at sub-millimeter wavelengths. As is the case for electrical crosstalk (see Section 2.1.1), analysis of the spectrometer data from the early phases of the mission has shown little evidence for this phenomenon. This lack of evidence notwithstanding, this processing module is retained in the spectrometer pipeline, but applies a null correction to the spectra.

3. CREATION OF LEVEL-2 SPECTRAL PRODUCTS

The final phase of the SPIRE spectrometer pipelines involves operations that modify the Level-1 spectrometer detector spectra produced by the building block pipeline to create a set of Level-2 spectral products. The format and the contents of the Level-2 spectral products depend on the observation: a point source spectrum product that contains the spectra for a single detector in each spectrometer array is produced for single pointing sparse sampling observations (see Section 3.1); a hyperspectral cube that contains two regularly spaced spatial dimensions and one spectral dimension per pixel is produced for all raster and jiggle mapping observations (see Section 3.2).

3.1 Single Pointing Sparse Sampling Observations

3.1.1 Point Source Spectral Response Correction and Flux Conversion

The purpose of this processing step is essentially the same as the relative response correction and flux conversion step in the building block pipeline (see Section 2.5.2). A separate and distinct correction for point source observations is required as the correction applied in the building block pipeline is appropriate for uniform, extended sources. In effect, this step applies the inverse of the extended source correction and then multiplies the input spectra by a wavenumber-dependent correction applicable to point-like astronomical sources:

$$I_{16-i}(\sigma) = I_{15-i}(\sigma) \times \frac{RSRF_{i-Extended}(\sigma)}{f_{i-Extended}(\sigma)} \times \frac{f_{i-Point}(\sigma)}{RSRF_{i-Point}(\sigma)}. \quad (25)$$

The conversion curves, $f_{i\text{-}Point}(\sigma)/RSRF_{i\text{-}Point}(\sigma)$, are derived from the results of an observation of Uranus and a model of its brightness[13]. The final Level-2 point source spectrum product contains spectra for only the central detectors of each array.

3.2 Mapping Observations

3.2.1 Spatial Regridding

The Level-1 spectral products created by the spectrometer building block pipeline contain one spectrum per detector. The spatial distribution of the spectra in the astronomical region of interest is determined by the hexagonally closed packed format of the detector arrays (Figure 5a).

For all SPIRE spectrometer mapping observations -- all raster observations and/or those performed at intermediate or full spatial sampling (Figure 5b, Figure 5c) -- the spatial regridding step interpolates the set of Level-1 SDS products

onto a hyperspectral data cube that is equidistantly sampled in the two spatial dimensions while leaving the equidistant grid along the spectral dimension unchanged.

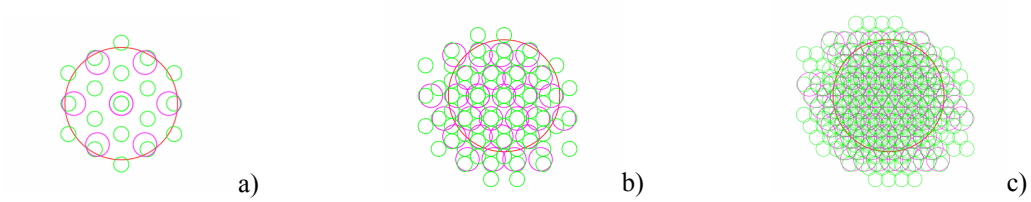

Figure 5: Astronomical footprint of the SPIRE detector arrays for the image sampling modes[3]: a) sparse sampling; b) intermediate sampling; c) full sampling. SSW detectors are represented by the small circles, SLW detectors are represented by the larger circles. The single large circle in each plot represents the 2 arcmin field of view that is covered by the unvignetted detectors.

The process of regridding the Level-1 spectral data involves first the creation of a suitable target grid in coordinates of Right Ascension and Declination. The pixel size within this target grid depends on the spatial sampling of the observation and is given in Table 1. Finally, the spectrum in each pixel of the target spatial grid is determined through a strict nearest-neighbor interpolation; the spectrum within a given pixel is given by the Level-1 spectrum whose spatial coordinates are closest to that pixel.

Alternate algorithms that take into account redundant spectra within a given pixel or take into account spectral uncertainties spectrum into account are under development and evaluation. In-flight measurements have shown that the size of the beam of the SPIRE spectrometer detectors vary in a non-linear fashion as a function of frequency between a full width at half maximum of 16.8-21.1 arcsec for SSW and 29.2-42.0 arcsec for SLW[3],[11]. Future regridding algorithms may also benefit from taking such the frequency-dependent beam sizes into account.

4. CONCLUSIONS

We have presented an update to the data processing pipelines for the SPIRE Imaging Fourier transform spectrometer. The data processing modules that are contained within these pipelines and the manner by which they are combined within the pipeline have been described with a special emphasis on those steps that have changed since the launch of the Herschel Observatory. The Level-0.5 and Level-1 building block data products, as well as the Level-2 point source spectrum and hyperspectral cube data products, for the SPIRE astronomical observation templates have been presented.

The transition from performance verification and science demonstration phases to routine operations for Herschel in general and the SPIRE spectrometer in particular mark a significant milestone in the mission. Analysis of the data from these early mission phases has resulted in many improvements to the processing. Further improvements to the data processing steps are expected to continue as more detailed knowledge of the behavior of the SPIRE FTS is gained throughout the mission.

ACKNOWLEDGEMENTS

The authors wish to acknowledge Karim Ali, Alim Harji, Yan He, Peter Kennedy, Joshua Litven, Cristian Merli, Andres Rebolledo, Yufei Ren, David Sharpe, Everett Sochowski, Dmitry Tebaykin, Zhaohan Weng, Yu Wai Wong, and Wilson Tzou for their contributions to the development of the SPIRE spectrometer data processing modules. The authors would also like to thank Christophe Ordenovic for his contributions to the first-level deglitching and telescope/instrument corrections. The figures that show the SPIRE astronomical footprint for the different spatial sampling modes were provided by Ivan Valtchanov. The funding for the Canadian contribution to SPIRE was provided by the Canadian Space Agency and NSERC.

REFERENCES

[1] Pilbratt, G. L., "The ESA Herschel Space Observatory: first year achievements and early science results," in Space Telescopes and Instrumentation I: Optical, Infrared, and Millimeter Wave (this volume), 7731-506, Proc. SPIE, (2010).

[2] Griffin, M. J., et. al., "Herschel-SPIRE: design, in-flight performance and scientific capabilities," in Space Telescopes and Instrumentation I: Optical, Infrared, and Millimeter Wave (this volume), 7731-39, Proc. SPIE, (2010).

[3] Herschel Science Centre, "SPIRE Observer's Manual," HERSCHEL-HSC-DOC-0798, version 2.0 (2010).

[4] Dowell, D., et. al., "Status of the SPIRE photometer data processing pipeline during the early phases of the Herschel Mission," in Space Telescopes and Instrumentation I: Optical, Infrared, and Millimeter Wave (this volume), 7731-112, Proc. SPIE, (2010).

[5] Ordenovic, C., Surace, C., Torresani, B. and Llebaria, A., "Glitches detection and signal reconstruction using Holder and wavelet analysis," ADAIV preprint, (2007).

[6] Cara, C., "Herschel SPIRE Detector Control Unit Design Document,", SPIRE-SAP-PRJ-001243, Tech. Rep., (2005).

[7] Davis-Imhof, P., et. al., "Deglitching SPIRE Interferograms," SPIRE-BSS-DOC-003195, version 0.5 (2008).

[8] Blackman, R. B. and Tukey, J. W., "Particular Pairs of Windows." In The Measurement of Power Spectra, From the Point of View of Communications Engineering. New York: Dover, 98-99 1959.

[9] Naylor, D. A. and Tahic, M. K., "Apodizing functions for Fourier transform spectroscopy," J. Opt. Soc. Am. A 24, 3644-3648 (2007).

[10] Naylor, D. A., et. al., "In-orbit performance of the Herschel/SPIRE imaging Fourier transform spectrometer," in Space Telescopes and Instrumentation I: Optical, Infrared, and Millimeter Wave (this volume), 7731-41, Proc. SPIE, (2010).

[11] Ferlet, M., "In-flight characterisation of Herschel-SPIRE optical performances," in Space Telescopes and Instrumentation I: Optical, Infrared, and Millimeter Wave (this volume) , 7731-111, Proc. SPIE, (2010).

[12] Fischer, J. et al., "Cryogenic far-infrared laser absorptivity measurements of the Herschel Space Observatory telescope mirror coatings," Applied Optics, 43, 3765 (2004).

[13] Griffin, M.J. & Orton, G.S., " The Near Millimeter Brightness Temperature Spectra of Uranus and Neptune," Icarus, 105, 537, (1993).